Journal of Hazardous Materials A114 (2004) 1–13

Journal of Hazardous Materials

www.elsevier.com/locate/jhazmat

Thermal reactive hazards of HMX with contaminants

Deng-Jr Peng[a], Cheng-Ming Chang[a,*], Miin Chiu[b]

[a] *Division of Occupational Safety, Institute of Occupational Safety and Health, Council of Labor Affairs, Executive Yuan, No. 99, Lane 407, Hengke Road, Shijr City, Taipei 221, Taiwan, ROC*

[b] *Department of Occupational Safety and Hygiene, Tajen Institute of Technology, No. 20, Wei-Hsin Road, Yenpu Shiang, Pingtung 907, Taiwan, ROC*

Received 29 December 2003; received in revised form 15 July 2004; accepted 18 August 2004

Abstract

In the past, many unexpected runaway accidents occurred in manufacturing processes, involving volatile chemical and explosive storage and transportation. Incompatible product reactions of high explosives must be carefully considered using loss prevention strategies for thermal hazards risk analysis. High explosive reactions vary via environmental changes, contact materials, or process situations, such as onset temperature and shifts in reaction type when high explosives are in contact with contaminants. Therefore, the manufacture and handling of high explosives require the utmost in safety and loss prevention.

HMX (cyclotetramethyene tetranitramine) is one kind of high explosive widely used around the world which is stable with high detonation strength properties. In this study, the influences of contaminants on HMX are investigated. The studied contaminants include ferrous chloride tetrahydrate, ferric chloride hexahydrate, acetone solution, acetic acid, and nitric acid. DSC thermal curves and incompatible reaction kinetic evaluations were preformed using iron, chlorine and acid. Organic acetone solution has lesser effects on HMX. Hopefully, this study will lead to improved thermal hazards risk analysis and reduce accidents.

Keywords: Unexpected runaway; Thermal hazard risk; Incompatible reaction; Contaminants; HMX

1. Introduction

Historically, high explosive explosions have occurred during storage, transportation or manufacturing processes, as listed in Table 1 [1,2]. Many explosive accident cases are negative publicized due to national security concerns. The causes of these accidents might occur because of discharged reactants or catalysts, incompatible component reactions and so on. Incompatible reactions shift the basic raw material characteristics and reaction profiles. For instance, the onset reaction temperature, time, enthalpy, kinetics and unexpected heat release are characteristics that could change due to incompatible reactions. Thus, it is imperative to prevent potential incompatible high explosive hazards.

In the past, the common high explosives were TNT (trinitrotoluene), RDX (cyclo-trimethylenetriamine or Hexogen) and HMX (cyclotetramethyene tetranitramine). After World War II, HMX became widely applied. The HMX molecular structure has three types of four polymorphs: β-form (stable at ambient temperature), α-form (stable between 337 and 429 K) and γ-form (stable above 429 K) [3]. In the past, many isothermal and non-isothermal techniques were applied in the study of HMX kinetic and chemical properties. Few studies investigated HMX incompatible reaction phenomena.

Based on the past operating experience and HMX production environments, HMX has opportunity to contact with contaminants such as ferrous chloride tetrahydrate, ferric chloride hexahydrate, acetone solutions, acetic acid and nitric

* Corresponding author. Tel.: +886 2 2660 7600x225; fax: +886 2 2660 7732.
E-mail address: ming@mail.iosh.gov.tw (C.-M. Chang).

0304-3894/$ – see front matter © 2004 Elsevier B.V. All rights reserved.
doi:10.1016/j.jhazmat.2004.08.029

Nomenclature

A	frequency factor for pure HMX or HMX mixed with contaminants reaction (s^{-1})
E_a	activation energy of pure HMX or HMX mixed with contaminants reaction (kJ mol^{-1})
$(dH/dt)_1$	enthalpy difference rate at reaction temperature 1 (kJ mol^{-1} min^{-1})
$(dH/dt)_2$	enthalpy difference rate at reaction temperature 2 (kJ mol^{-1} min^{-1})
$(dH/dt)_3$	enthalpy difference rate at reaction temperature 3 (kJ mol^{-1} min^{-1})
ΔH	enthalpy reaction differences (kJ mol^{-1})
ΔH_1	enthalpy difference at reaction temperature 1 (kJ mol^{-1})
ΔH_2	enthalpy difference at reaction temperature 2 (kJ mol^{-1})
ΔH_3	enthalpy difference at reaction temperature 3 (kJ mol^{-1})
m	sample mass (mg)
n	order of pure HMX or HMX mixed with contaminants reaction
Q_{max}	maximum heat flow of DSC thermal curves (mW)
r	heating rate of DSC experiment (°C/min)
R	universal gas constant (J mol^{-1} K^{-1})
T	temperature of reaction in DSC experiment (°C or K)
T_0	onset temperature of reaction (°C or K)
T_1	reaction temperature 1 of DSC dynamic test (K)
T_2	reaction temperature 2 of DSC dynamic test (K)
T_3	reaction temperature 3 of DSC dynamic test (K)
T_p	temperature of peak in DSC thermal curves (°C or K)

Greek letter

γ	correction coefficient for linear regression

Subscripts

1	condition in reaction 1
2	condition in reaction 2
3	condition in reaction 3
4	condition in reaction 4
endo	endothermic reaction
exo	exothermic reaction

acid in the manufacturing process. This study investigated the influences of incompatible HMX reactions with the aforementioned contaminants using DSC (differential scanning calorimetry) dynamic thermal analysis.

2. Experimental

2.1. High explosive β-form HMX

Pure HMX was provided directly from the manufacturer. The produced HMX was in β-form with high stable chemical properties but larger heat release. The mass of the pure HMX sample ranged between 1.5 ± 0.1 mg.

2.2. Contaminants

The ferrous chloride tetrahydrate (15 wt.%), ferric chloride hexahydrate (40 wt.%) and acetone (100 wt.%) were purchased from Merck & Co. Inc. The acetic acid (100 wt.%) and nitric acid (100 wt.%) used to produce β-form HMX in the actual process were provided directly from the manufacturer. The contaminant sample masses used were between 1.5 ± 0.1, respectively.

2.3. Instrument

Incompatible reaction determination was conducted using Mettler Toledo DSC 822^e differential scanning calorimetry. The heating rates used in the dynamic scanning experiments were 1, 2, 4 and 10 °C/min to calculate the HMX and contaminant reaction heat, thermal curves, activity energy and frequency factors.

2.4. Analysis

The mixed pure HMX and contaminant test weight mix ratio was 1:1. During the HMX manufacturing process, ferrous chloride tetrahydrate and ferric chloride hexahydrate could come in contact with the HMX product via pipeline construction materials, reactor wall, fixed valves, and the dissolved chlorine used to disinfect the water. In addition, acetone solvent is used to separate reactive products, RDX (cyclo-trimethylenetriamine, Hexogen), that have the capacity to affect HMX. Both acetic and nitric acids are reactants in the HMX manufacturing process. This study used the 'quality not quantity approach' to determine HMX contaminant incompatible reaction phenomena.

3. Results and discussion

The DSC thermal curves for pure HMX used heating rates of 1, 2, 4 and 10 °C/min in the DSC device. Endothermic phase transitions in the 183.97–195.59 °C temperature range from −2.06 to −25.41 J/g endothermic heats are presented in Fig. 1. The thermal curves show a very strong and sharp exothermic peak that released 2 883.54–4 226.20 J/g heat along with peak temperatures of 268.77, 275.48, 291.92 and 292.58 °C at heating rates of 1, 2, 4 and 10 °C/min, respectively. The onset temperature range was from 265.54–279.04 °C. The DSC experimental data for pure

Table 1
High explosive explosion cases list since 1916–1996 [1,2]

Date	Location	Plant/transport	Chemical	Deaths/injuries
1916	New York, USA	Barge, rail cars	Explosives	5/many
1917	Ashton/UK	Chemical works	–	46/120
1917	Nova Scotia, Canada	Ship	Munitions	1963/≒8000
1917	Silvertown, UK	Munitions works	TNT	69/≒426
1944	Fauld, UK	Munitions store	Munitions	68/22
1956	Cali, Columbia	Road vehicle	Dynamite, munitions	≒1200 deaths
1971	Georgia, USA	Road vehicle	Explosives	5/33
1973	Arkansas, USA	Rail cars	Munitions	–
1980	Gach Saran, Iran	Warehouse	Nitroglycerine	80/45
1988	Arzamas, USSR	Railway station	Explosives	73/230
1991	Liaoning, China	Manufacturing plant	Trinitrotoluene	17/107
1992	Hubei, China	Chemical factory	Nitroamine	22/13
1993	Shenzhen, China	Warehouse	Ammonium nitrate	15/141
1994	Shandong, China	Road vehicle	Detonators	5/95
1996	Hunan, China	Manufacturing plant	Cyclo-trimethylenetriamine	134/117

HMX and contaminants are shown in Table 2. Heating rates of 1, 2, 4 and 10 °C/min were used. Observed from these thermal curves, the onset temperature, maximum heat flow and reaction heat could be shifted by different heating rates. Accordingly, the heating rate influence was considered in the incompatible experiments. The following discussions investigate the HMX contaminant reaction phenomena accompanied with the effects of a variety of heating rates.

3.1. Ferrous chloride tetrahydrate and HMX mixtures

The DSC thermal curves in Fig. 2 present the HMX incompatible reaction with ferrous chloride tetrahydrate dry mixtures at heating rates of 1, 2, 4 and 10 °C/min^{-1}. Compared with the reaction capacities of pure HMX, the ferrous chloride tetrahydrate mixtures advanced the initial exothermic heat release temperature by approximately 75–90 °C. The heat release reaction was separated into two (while heating rates are 2, 4 and 10 °C/min^{-1}) or three stages (at heating rate 1 °C). The secondary exothermic heat release temperature increased from 219.75 to 358.44 °C via increased heating rates, as shown in Table 3. Compared with different heating rates, the lowest 1 °C/min caused the most unstable ferrous chloride tetrahydrate reaction. The HMX endothermic phase transition disappeared, while the ferrous chloride tetrahydrate endothermic phenomena was still present at a temperature range from 76.31 to 82.26 °C. Thus, ferrous chloride tetrahydrate shifts the HMX in the reaction.

3.2. Ferric chloride hexahydrate and HMX mixtures

The DSC thermal curves in Fig. 3 show the ferric chloride hexahydrate mixed with pure HMX reaction phenomena. The initial exothermic heat release temperature occurred at a range from 172.00 to 182.76 °C. The total heat released is shown in Table 4 using heating rates of 1, 2, 4 and 10 °C/min. Compared with the pure HMX reaction, the heat release temperature was advanced, and the released heat decreased. The

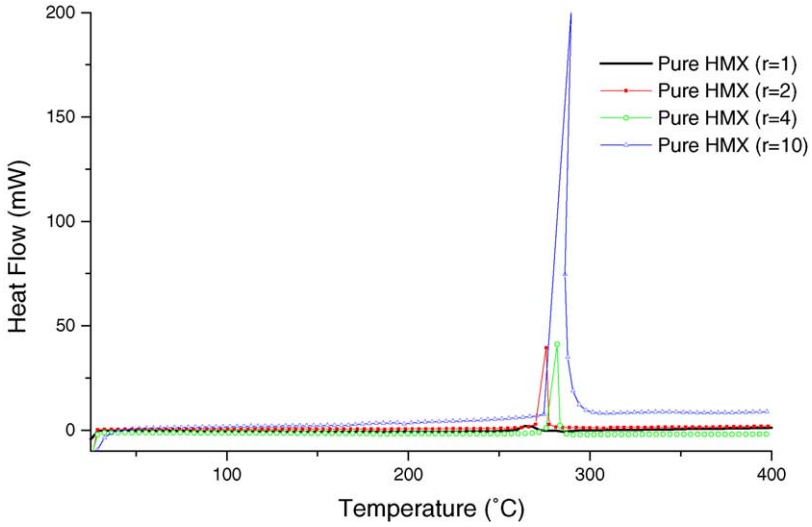

Fig. 1. Heat flow vs. temperature plot for DSC dynamic experiments for pure HMX at a scanning rate of 1, 2, 4 and 10 °C/min.

Table 2
Summarized results for DSC experiments of pure HMX and contaminants

r (°C/min)	m (mg)	Endothermic peaks								Exothermic peaks					
		$T_{0,1}$ (°C)	ΔH_1 (J g^{-1})	$T_{0,2}$ (°C)	ΔH_2 (J g^{-1})	$T_{0,3}$ (°C)	ΔH_3 (J g^{-1})	$T_{0,4}$ (°C)	ΔH_4 (J g^{-1})	$T_{0,1}$ (°C)	ΔH_1 (J g^{-1})	$T_{0,2}$ (°C)	ΔH_2 (J g^{-1})	$T_{0,3}$ (°C)	ΔH_3 (J g^{-1})
1	HMX 1.6	183.97	−25.41	–	–	–	–	–	–	265.54	2883.54	–	–	–	–
	$FeCl_2{\cdot}4H_2O$ 1.5	76.31	−63.72	233.6	−1.7	292.05	−51.15	306.45	−188.61	–	–	–	–	–	–
	$FeCl_3{\cdot}6H_2O$ 1.5	33.16	−94.25	297.01	−354.81	–	–	–	–	–	–	–	–	–	–
	$CH_3COCH_3$1.5	–	–	–	–	–	–	–	–	285.30	300.01	–	–	–	–
	CH_3COOH 1.6	–	–	–	–	–	–	–	–	214.53	29.96	–	–	–	–
	$HNO_3$1.6	295.77	−33.33	–	–	–	–	–	–	177.01	355.25	300.78	153.66	–	–
2	HMX 1.5	184.95	−10.75	–	–	–	–	–	–	272.48	2954.44	–	–	–	–
	$FeCl_2{\cdot}4H_2O$ 1.4	76.74	−95.45	238.17	−27.40	317.53	−21.01	351.41	−163.79	–	–	–	–	–	–
	$FeCl_3{\cdot}6H_2O$ 1.5	33.50	−55.45	321.87	−291.60	–	–	–	–	–	–	–	–	–	–
	$CH_3COCH_3$1.6	–	–	–	–	–	–	–	–	169.30	2.65	261.40	134.90	365.56	15.16
	CH_3COOH 1.4	–	–	–	–	–	–	–	–	253.33	53.74	–	–	–	–
	$HNO_3$1.5	99.93	−26.60	124.01	−47.96	171.09	−553.20	–	–	282.68	94.54	–	–	–	–
4	HMX 1.4	185.87	−25.20	–	–	–	–	–	–	277.25	4226.20	–	–	–	–
	$FeCl_2{\cdot}4H_2O$ 1.5	78.65	−76.05	236.22	−13.11	283.59	−45.45	354.98	−147.46	–	–	–	–	–	–
	$FeCl_3{\cdot}6H_2O$ 1.5	34.29	−39.66	283.76	−503.24	–	–	–	–	–	–	–	–	–	–
	$CH_3COCH_3$1.5	–	–	–	–	–	–	–	–	94.88	2.02	174.12	31.52	272.51	29.53
	CH_3COOH 1.4	–	–	–	–	–	–	–	–	237.29	136.74	–	–	–	–
	$HNO_3$1.5	186.79	−155.44	239.08	−66.38	–	–	–	–	321.93	550.11	–	–	–	–
10	HMX 1.5	195.59	−2.06	–	–	–	–	–	–	279.04	3368.05	–	–	–	–
	$FeCl_2{\cdot}4H_2O$ 1.6	82.26	−84.51	240.00	−6.11	366.65	−172.58	–	–	–	–	–	–	–	–
	$FeCl_3{\cdot}6H_2O$ 1.6	37.17	−6.93	325.18	−268.57	379.03	−4.37	–	–	–	–	–	–	–	–
	$CH_3COCH_3$1.5	–	–	–	–	–	–	–	–	100.05	4.5	184.51	142.50	282.16	37.53
	CH_3COOH 1.6	–	–	–	–	–	–	–	–	247.89	137.56	–	–	–	–
	$HNO_3$1.5	168.51	−9.62	203.33	−147.87	247.24	−19.57	270.82	−14.61	327.62	439.63	–	–	–	–

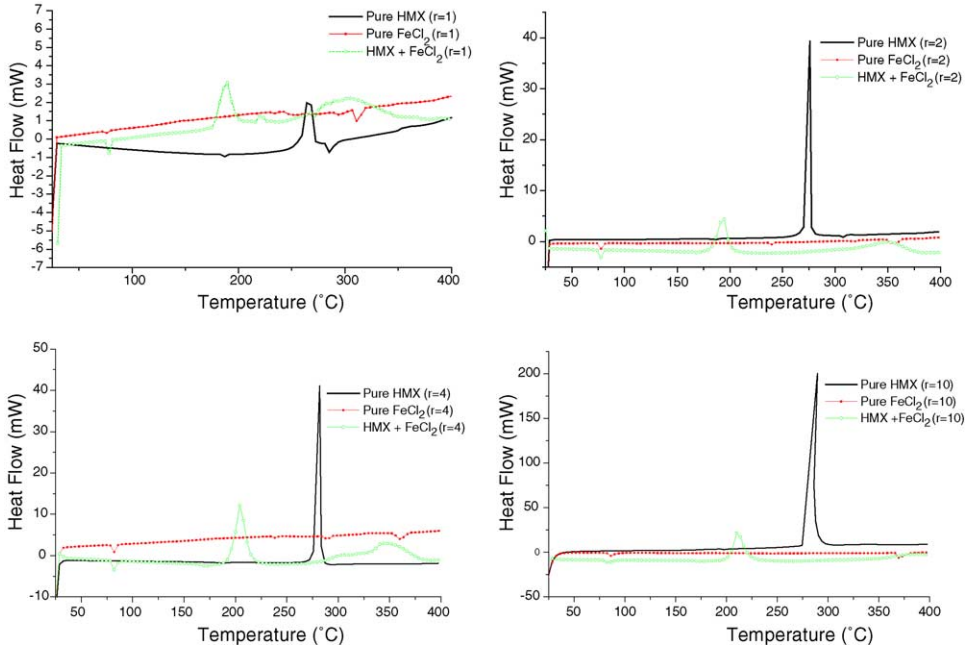

Fig. 2. Heat flow vs. temperature plot for DSC dynamic experiments for HMX mixed with ferrous chloride tetrahydrate at a scanning rate of (a) 1, 2 and 4 °C/min and (b) 10 °C/min.

HMX endothermic phase transition disappeared, while the ferric chloride hexahydrate endothermic capacity remained after the heat release peak. In addition, the ferric chloride hexahydrate and HMX mixture reaction exhibited most unstable heating rate capacity, 1 °C/min. The secondary exothermic peak occurred while the heating rate was increased. Therefore, ferric chloride hexahydrate influences HMX reaction.

3.3. Acetone solution and HMX mixtures

Based on the DSC thermal curves, the HMX acetone solution mixture reaction is presented in Fig. 4. Acetone solution advanced the initial HMX exothermic heat release temperature from 15 to 43 °C. The amount of heat released decreased by approximately 1400–2400 J/g, was shown in

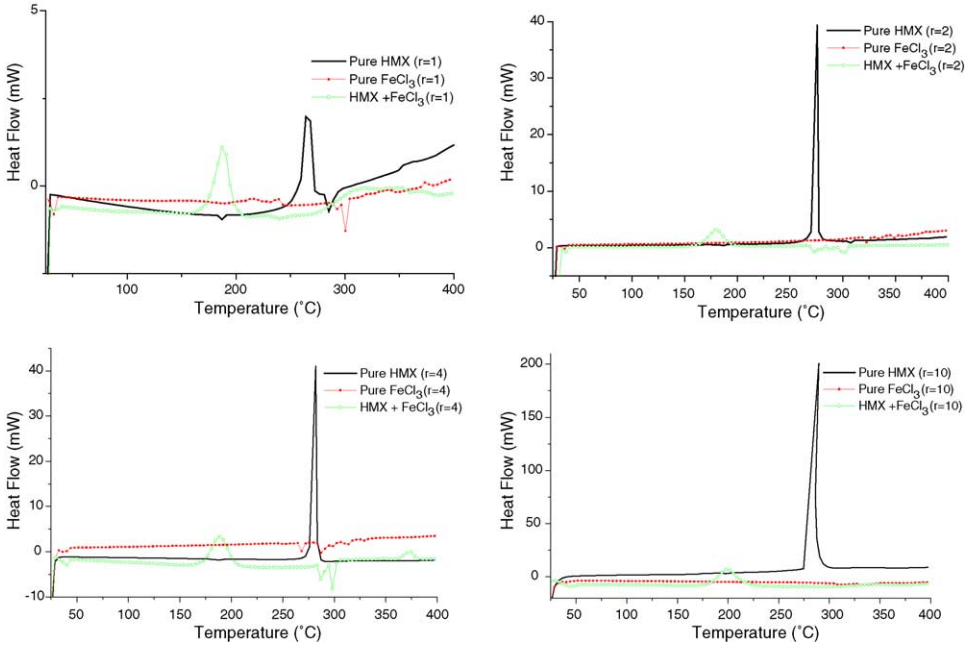

Fig. 3. Heat flow vs. temperature plot for DSC dynamic experiments for HMX mixed with ferric chloride hexahydrate at a scanning rate of 1, 2, 4 and 10 °C/min.

Table 3
Summarized results for DSC experiments of ferrous chloride tetrahydrate mixed with HMX

Sample	r (°C/min)	m (mg)	$T_{0,endo}$ (°C)	ΔH_{endo} (J g^{-1})	$T_{0,exo,1}$ (°C)	$T_{P,exo,1}$ (°C)	$Q_{max,1}$ (mW)	$\Delta H_{exo,1}$ (J g^{-1})	$T_{0,exo,2}$ (°C)	$T_{P,exo,2}$ (°C)	$Q_{max,2}$ (mW)	$\Delta H_{exo,2}$ (J g^{-1})	$T_{0,exo,3}$ (°C)	$T_{P,exo,3}$ (°C)	$Q_{max,3}$ (mW)	$\Delta H_{exo,3}$ (J g^{-1})
HMX + $FeCl_2{\cdot}4H_2O$	1	HMX: 1.6 $FeCl_2{\cdot}4H_2O$: 1.5	76.16	−36.48	173.74	188.18	2.44	547.34	219.75	220.23	0.70	41.92	266.63	304.56	0.91	810.55
HMX + $FeCl_2{\cdot}4H_2O$	2	HMX: 1.5 $FeCl_2{\cdot}4H_2O$: 1.5	75.13	−51.48	187.12	192.99	8.08	813.33	314.25	349.23	2.11	1063.77	–	–	–	–
HMX + $FeCl_2{\cdot}4H_2O$	4	HMX: 1.5 $FeCl_2{\cdot}4H_2O$: 1.5	79.33	−47.69	196.53	204.61	14.34	902.59	330.14	346.52	3.41	613.08	–	–	–	–
HMX + $FeCl_2{\cdot}4H_2O$	10	HMX: 1.5 $FeCl_2{\cdot}4H_2O$: 1.5	79.23	−46.53	204.63	210.96	32.25	862.14	358.44	379.32	1.78	85.12	–	–	–	–

Table 4
Summarized results for DSC experiments of ferric chloride hexahydrate mixed with HMX

Sample	r (°C/min)	m (mg)	$T_{0,endo}$ (°C)	ΔH_{endo} (J g^{-1})	$T_{0,exo,1}$ (°C)	$T_{P,exo,1}$ (°C)	$Q_{max,1}$ (mW)	$\Delta H_{exo,1}$ (J g^{-1})	$T_{0,exo,2}$ (°C)	$T_{P,exo,2}$ (°C)	$Q_{max,2}$ (mW)	$\Delta H_{exo,2}$ (J g^{-1})	$T_{0,endo,1}$ (°C)	$\Delta H_{endo,1}$ (J g^{-1})	$T_{0,endo,2}$ (°C)	$\Delta H_{endo,2}$ (J g^{-1})
HMX + $FeCl_3{\cdot}6H_2O$	1	HMX: 1.5 $FeCl_3{\cdot}6H_2O$: 1.6	31.78	−11.37	180.91	187.84	1.95	572.12	–	–	–	–				
HMX + $FeCl_3{\cdot}6H_2O$	2	HMX: 1.5 $FeCl_3{\cdot}6H_2O$: 1.4	34.04	−29.09	172.00	179.98	3.10	579.19	–	–	–	–	276.26	−118.25	295.28	−128.93
HMX + $FeCl_3{\cdot}6H_2O$	4	HMX: 1.5 $FeCl_3{\cdot}6H_2O$: 1.6	32.88	−46.99	173.96	188.16	6.47	632.85	363.84	373.14	1.72	92.07	286.76	−70.72	295.57	−184.97
HMX + $FeCl_3{\cdot}6H_2O$	10	HMX: 1.5 $FeCl_3{\cdot}6H_2O$: 2.5	35.27	−77.38	182.76	199.02	15.81	760.52	319.78	340.38	1.14	63.71	–	–	–	–

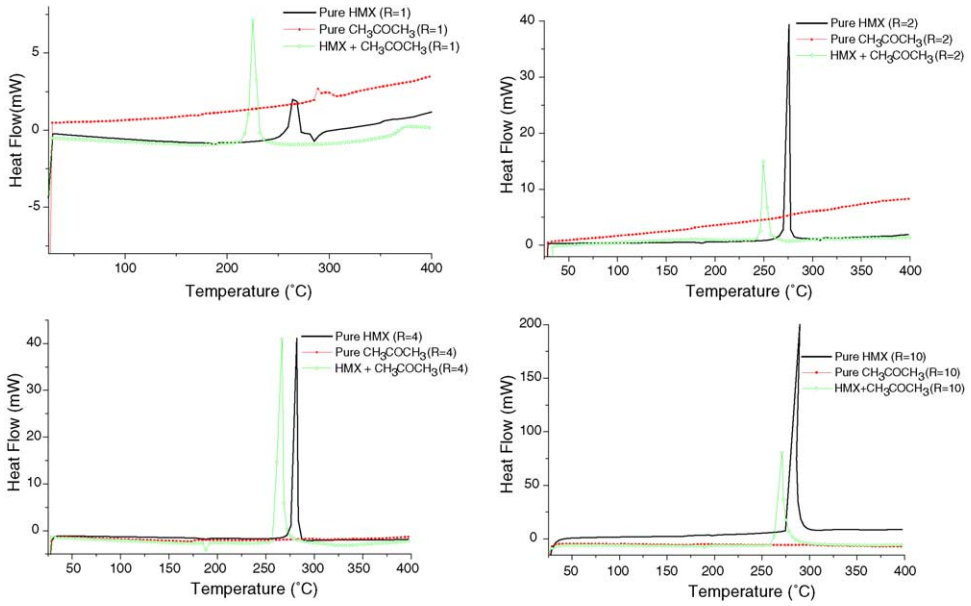

Fig. 4. Heat flow vs. temperature plot for DSC dynamic experiments for HMX mixed with acetone at a scanning rate of (a) 1, 2, 4 °C/min and (b) 10 °C/min.

Table 5. From the incompatible acetone solution and HMX mixture experiments, acetone solution is a safe solvent for use in HMX storage and operation usage. However, the initial exothermic heat release temperature is cautiously monitored.

3.4. Acetic acid and HMX mixtures

Observed from the DSC thermal curves at heating rates of 1, 2, 4 and 10 °C/min Fig. 5 presents the reaction capacities of acetic acid solution mixed with HMX. Acetic acid

Table 5
Summarized results for DSC experiments of acetone mixed with HMX

Sample	r (°C/min)	m (mg)	$T_{0,endo}$ (°C)	ΔH_{endo} (J g^{-1})	$T_{0,exo,1}$ (°C)	$T_{P,exo,1}$ (°C)	$Q_{max,1}$ (mW)	$\Delta H_{exo,1}$ (J g^{-1})
HMX + CH_3COCH_3	1	HMX: 1.5 Acetone: 1.4	–	–	222.71	227.24	13.76	1500.34
HMX + CH_3COCH_3	2	HMX: 1.5 CH_3COCH_3: 1.6	197.99	−18.89	248.38	250.31	24.69	1846.84
HMX + CH_3COCH_3	4	HMX: 1.5 CH_3COCH_3: 1.5	187.85	−10.79	264.30	267.42	82.72	1497.12
HMX + CH_3COCH_3	10	HMX: 1.6 CH_3COCH_3: 1.5	186.53	−16.60	264.22	271.35	111.56	1531.69

Table 6
Summarized results for DSC experiments of acetic acid mixed with HMX

Sample	r (°C/min)	m (mg)	$T_{0,endo}$ (°C)	ΔH_{endo} (J g^{-1})	$T_{0,exo,1}$ (°C)	$T_{P,exo,1}$ (°C)	$Q_{max,1}$ (mW)	$\Delta H_{exo,1}$ (J g^{-1})	$T_{0,exo,2}$ (°C)	$T_{P,exo,2}$ (°C)	$Q_{max,2}$ (mW)	$\Delta H_{exo,2}$ (J g^{-1})
HMX + CH_3COOH	1	HMX: 1.5 CH_3COOH: 1.5	–	–	213.32	221.63	5.99	1200.24	361.87	364.61	1.04	163.89
HMX + CH_3COOH	2	HMX: 1.5 CH_3COOH: 1.6	179.05	−12.32	229.85	236.29	13.83	1164.76	–	–	–	–
HMX + CH_3COOH	4	HMX: 1.5 CH_3COOH: 1.5	182.38	−12.55	232.76	243.24	16.84	1199.46	–	–	–	–
HMX + CH_3COOH	10	HMX: 1.6 CH_3COOH: 1.5	183.09	−9.67	249.96	261.83	34.97	1292.14	–	–	–	–

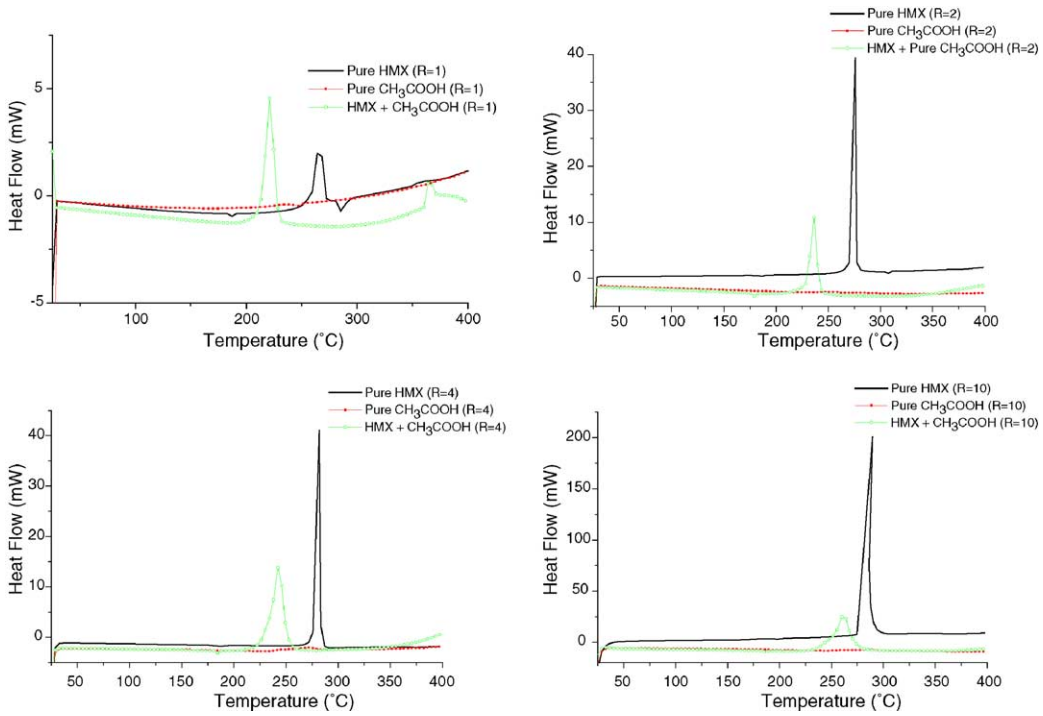

Fig. 5. Heat flow vs. temperature plot for DSC dynamic experiments for HMX mixed with acetic acid at a scanning rate of 1, 2, 4 and 10 °C/min.

also advanced the initial exothermic heat release temperature and decreased the released heat as shown in Table 6. In addition, the HMX endothermic phase transition disappeared while the heating rate decreased. The heat release phenomena separated into two stages. Therefore, when HMX is mixed with acetic acid, production operators should be cautious of any increase in the initial exothermic temperature or opportunity for secondary heat release.

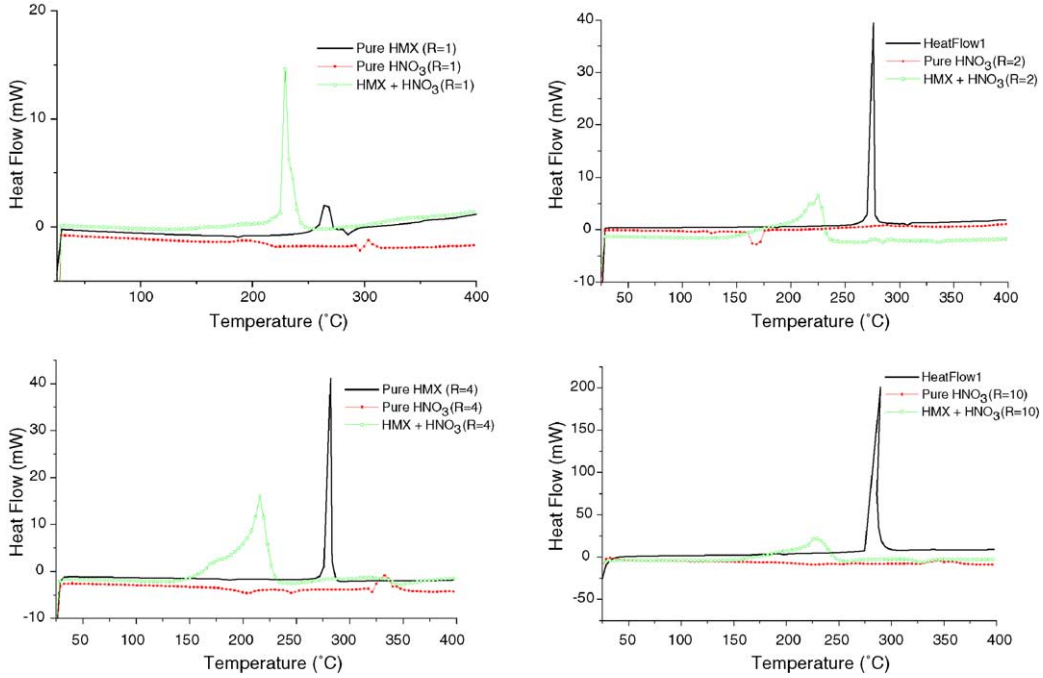

Fig. 6. Heat flow vs. temperature plot for DSC dynamic experiments for HMX mixed with nitric acid at a scanning rate of 1, 2, 4 and 10 °C/min.

Table 7
Summarized results for DSC experiments of nitric acid mixed with HMX

Sample	r (°C/min)	m (mg)	$T_{0,endo}$ (°C)	ΔH_{endo} (J g^{-1})	$T_{0,exo,1}$ (°C)	$T_{P,exo,1}$ (°C)	$Q_{max,1}$ (mW)	$\Delta H_{exo,1}$ (J g^{-1})	$T_{0,exo,2,3}$ (°C)	$T_{P,exo,2,3}$ (°C)	$Q_{max,2,3}$ (mW)	$\Delta H_{exo,2,3}$ (J g^{-1})	$T_{0,endo,1}$ (°C)	$\Delta H_{endo,1}$ (J g^{-1})	$T_{0,endo,2}$ (°C)	$\Delta H_{endo,2}$ (J g^{-1})
HMX + HNO_3	1	HMX: 1.5 $FeCl_3$: 1.5	165.32	−13.27	226.80	230.07	18.48	2101.89	–	–	–	–	–	–	–	–
HMX + HNO_3	2	HMX: 1.6 $FeCl_3$: 1.6	–	–	222.08	226.16	9.61	2813.54	270.47 and 285.19	277.53 and 290.89	0.55 and 0.47	47.34 and 38.37	332.05	−24.44		
HMX + HNO_3	4	HMX: 1.5 $FeCl_3$: 1.5	–	–	204.49	215.43	18.54	2679.85	–	–	–	–	290.45	−4.73	336.02	−152.05
HMX + HNO_3	10	HMX: 1.5 $FeCl_3$: 1.6	–	–	213.98	227.68	27.57	2197.59	–	–	–	–	318.47	−113.23	–	–

3.5. Nitric acid and HMX mixtures

According to the DSC thermal curves in Fig. 6, the apparent incompatibility effects of a HMX nitric acid solution were observed. The exothermic heat release peak exhibited a shoulder shape. The initial exothermic heat release temperature increased by approximately 50–60 °C, and the released heat decreased by a small amount as shown in Table 7. The HMX endothermic phase transition phenomenon disappeared, while another endothermic peak occurred after the heat release. Thus, nitric acid must be used cautiously in the HMX manufacturing process.

3.6. Kinetics evaluations

Because the main HMX with contaminant exothermic peak corresponds to the contaminant reactions with a synergetic heat release, the kinetic parameters videlicet, activation energy (E_a), frequency factor (A), and order of reaction(n), for these reactions were evaluated. The Kissinger, Ozawa and Freeman–Carroll's methods were employed using the DSC experimental data in Tables 2–7 at heating rates 1, 2, 4 and 10 °C/min.

3.6.1. Kissinger method [4]

The widely used Kissinger method is based on the plot of $\ln(r/T_P^2)$ versus $-1/T_P$, where 'r' is the heating rate and T_p the DSC absolute peak temperature. The activation energy and frequency factor values are calculated from Kissinger's plot with the equation as follows:

$$\ln\left(\frac{r}{T_P^2}\right) = \ln\left(\frac{AR}{T}\right) - \frac{E_a}{RT_P} \tag{1}$$

3.6.2. Ozawa method [5]

The Ozawa method used the plot of $\log r$ versus $-1/T_P$. The kinetic parameters were obtained from the following equation which has item $G(x_m) = (ART_P^2/rE_a)\exp(-E_a/RT_P)$:

$$\log r = -0.4567\frac{E_a}{RT_P} - 2.315 + \log\frac{AE_a}{R} - \log G(x_m) \tag{2}$$

3.6.3. Freeman–Carroll's approach [6]

Based on the Freeman–Carroll's approach, the reaction order using a DSC dynamic scanning experiment was determined via the following equation:

$$n = \frac{\begin{array}{c}(\log((\mathrm{d}H/\mathrm{d}t)_3/(\mathrm{d}H/\mathrm{d}t)_1)/(1/T_1 - 1/T_3)) \\ -(\log((\mathrm{d}H/\mathrm{d}t)_2/(\mathrm{d}H/\mathrm{d}t)_1)/(1/T_1 - 1/T_2))\end{array}}{\begin{array}{c}(\log(\Delta H_1/\Delta H_2)/(1/T_1 - 1/T_2)) \\ -(\log(\Delta H_1/\Delta H_3)/(1/T_1 - 1/T_3))\end{array}} \tag{3}$$

Table 8
Calculated kinetic parameters of HMX with contaminants

Sample	Kissinger method			Ozawa method			Freeman–Carroll's approach
	E_a (kJ/mole)	A (1/s)	γ^a	E_a (kJ/mole)	A (1/s)	γ^a	n^b
Pure HMX	236.97	1.63×10^{19}	0.9999	233.76	1.79×10^{19}	0.9999	1.002931515
HMX + $FeCl_2 \cdot 4H_2O$	175.02	1.96×10^{16}	0.9919	173.54	2.41×10^{16}	0.9924	0.9988257734
HMX + $FeCl_3 \cdot 6H_2O$	143.04	1.70×10^{13}	0.9999	143.10	2.57×10^{13}	0.9999	1.000146193
HMX + CH_3COCH_3	67.97	3.15×10^{3}	0.9854	72.95	1.12×10^{4}	0.9886	1.004555157
HMX + CH_3COOH	118.13	8.00×10^{8}	0.9970	120.28	1.61×10^{9}	0.9973	1.000965465
HMX + HNO_3	144.49	2.82×10^{12}	0.9999	144.73	4.31×10^{12}	0.9999	1.016923245

[a] γ: correction coefficient for linear regression.
[b] n: order of main exothermic reaction at heating rate 4 °C/min.

Eventually, the HMX with contaminant kinetic parameters are presented in Table 8. The HMX with contaminant activation energies and frequency factors both increased compared to pure HMX. This means that when HMX contacted a variety of contaminants, the reaction kinetic types could incur substantial changes, producing unstable conditions increasing the opportunity for hazards. In addition, the main exothermic reaction order has no significant change in the present calculated results. Incompatible HMX contaminant reactions did not change the main exothermic reaction order, but did change the reaction type (such as the shape of exothermic peak, etc.).

3.7. Proposed reaction mechanisms

According to the kinetic decomposition mechanisms proposed by Hobbs in 2002 [7], Fig. 7 illustrates the HMX reaction pathways. In his study, the HMX reaction was separated into two steps, Λ → δ and L → d, along with the increase in temperature.

The reaction Λ → δ was suggested to control the rate of decomposition. The intermediate products δ and d then combined with $CH_2O + N_2O$ to generate the final products H_2O, N_2 and CO. This was also verified by Kimura in 1980 [8]. In this study, the ferrous chloride tertrahydrate and ferric chloride hexahydrate contaminants produced similar reaction steps connecting the free electrons in δ as a catalyst to form the final products, as shown in Fig. 8. A HMX decomposition rate control reaction Λ → δ also occurred, but the intermediate product δ connected the ferrous chloride tertrahydrate and ferric chloride hexahydrate, to vary the reaction pathways.

Acetone solution could not offer protons due to the oxidizing agent. Accordingly, HMX mixed with acetone solution has no opportunity to produce an incompatible reaction. HMX mixed with acetic acid, CH_3COO^- and H_3O^+ were decomposed which offered a proton to connect the intermediate product δ from the Λ → δ reaction, whereas the L → d reaction did not occur. NO_2 accompanied with a positive charge was generated to result in the final products $(CH_2)_4N_4(NH)_4$, CH_3COOH and HNO_3, as presented in Fig. 9. Thus, the HMX reaction pathways varied from the NO_2 with positive charge effect. Nitric acid has analogous reaction pathways with acetic acid. After the decomposition reaction Λ → δ with HMX, the HNO_3 has an O–H bond broken to offer a proton to connect with the intermediate product δ and NO_3 accompanied with a negative charge to form the final products $(CH_2)_4N_4(NH)_4$ and N_2O_5, as shown in Fig. 10. All of the aforementioned reaction pathways were verified using analysis instruments, such as GC (gas chromatography) and HPLC (high performance liquid chromatography).

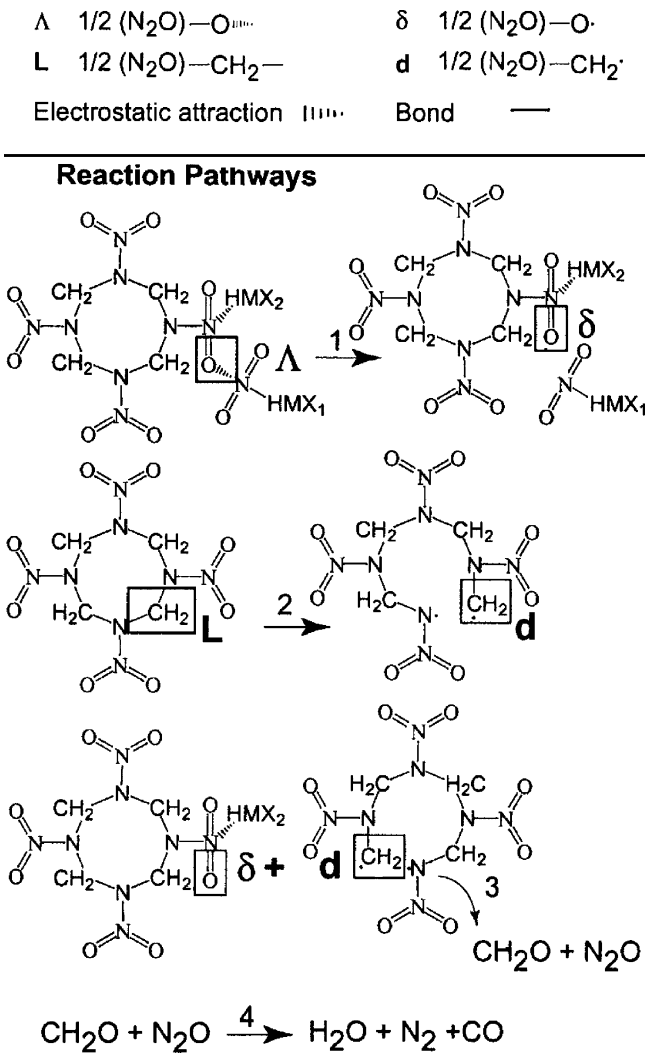

Fig. 7. Proposed kinetic decompose mechanisms for HMX [7].

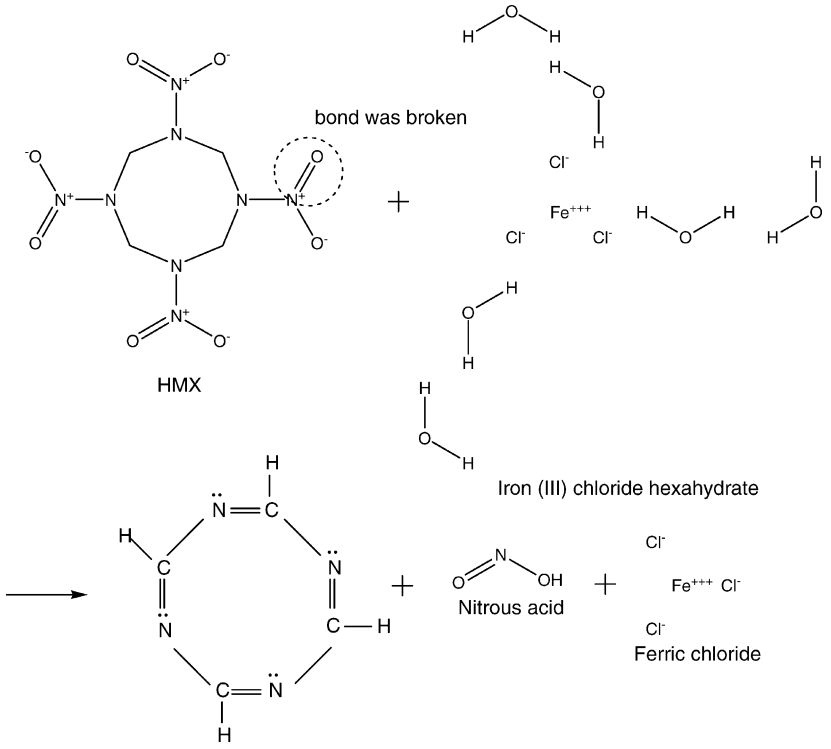

Fig. 8. Proposed overall kinetic decompose mechanism for HMX mixed with ferric chloride haxahydrate.

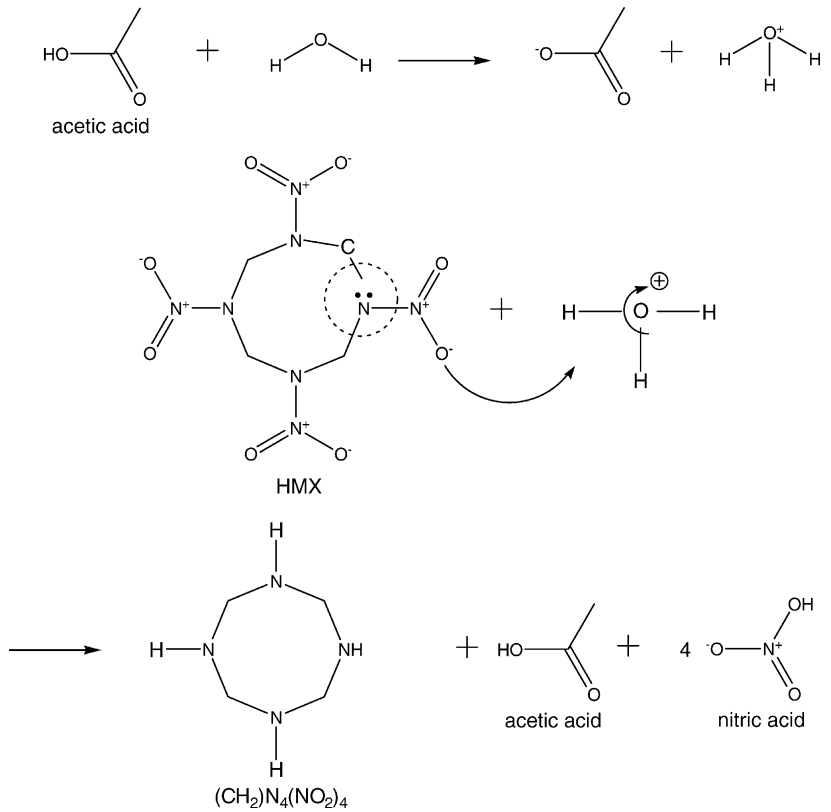

Fig. 9. Proposed overall kinetic decompose mechanism for HMX mixed with acetic acid.

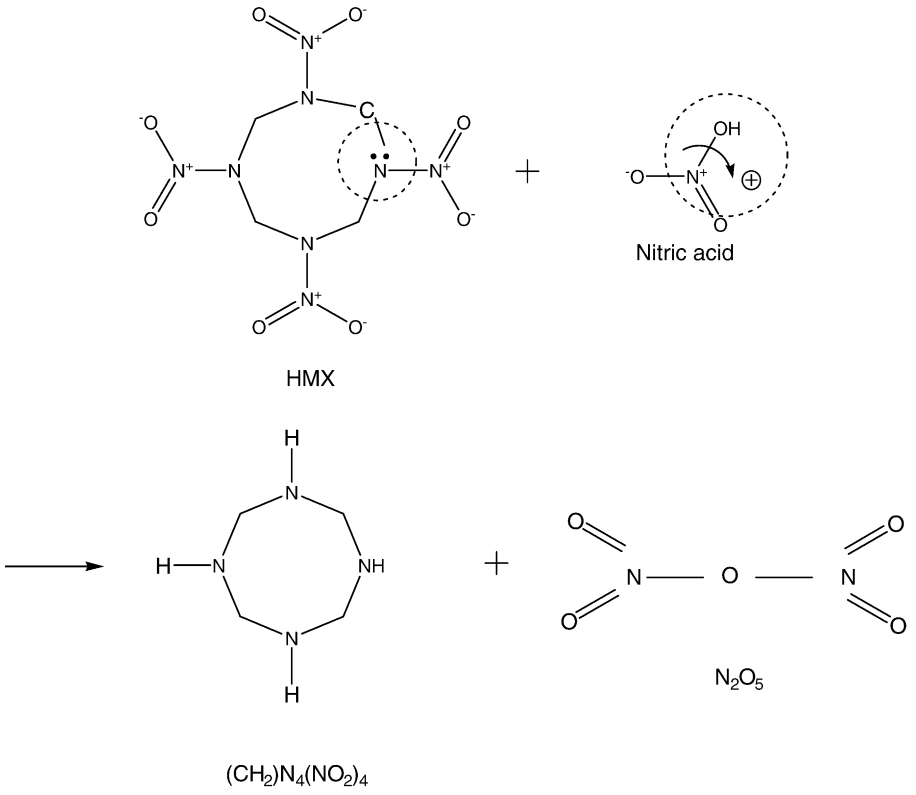

Fig. 10. Proposed overall kinetic decompose mechanism for HMX mixed with nitric acid.

4. Conclusion

Based on the discussed DSC experimental results, kinetic evaluations and proposed overall reaction mechanisms, this study presents the following suggestions:

- The heating rate influence on the thermal decomposition of HMX mixed with contaminants was an important factor. The heating rate used to conduct this investigation was 4 °C/min. The heating rate (1 °C/min) was not suggested because the rate induced unstable reactions.
- Ferrous chloride tetrahydrate, ferric chloride tetrahydrate and nitric acid induced the HMX endothermic peak to disappear and produced an automatic endothermic reaction.
- The exothermic reaction could be divided into two stages via ferrous chloride tetrahydrate, ferric chloride tetrahydrate and acetic acid. The main exothermic peak produced with nitric acid varied and exhibited a shoulder shaped profile.
- The thermodynamic properties (e.g., T_0, T_f, ΔH, etc.), kinetic parameters (e.g., E_a, A and n) and reaction pathways exhibited significant changes after HMX was mixed with ferrous chloride tetrahydrate, ferric chloride tetrahydrate, acetic acid and nitric acid.

The incompatible HMX with contaminant reactions influenced temperature control, heating and cooling systems, and produced a secondary unexpected explosion. This is a serious potential hazard. Hopefully, this study has highlighted the incompatible risks involved with contaminated HMX during production, handling, transportation and storage.

Acknowledgements

The authors appreciate the support provided by The Institute of Occupational Safety and Health, Council of Labor Affairs, Executive Yuan, under Grant No. IOSH92-S308, 203 Rd, Arsenal Material Production Service and Dr. Kwan-Hua Hu who provided valuable help in this study.

References

[1] G. Zhang, Causes and lessons of five explosion accidents, J. Loss Prev. Proc. Ind. 13 (2000) 439.
[2] F.P. Lees, Loss Prevention in the Process Industries, second ed., Oxford, UK, 2001.
[3] E.S. Kim, H.S. Lee, C.F. Mallery, S.T. Thynell, Thermal decomposition studies of energetic materials using confined rapid thermolysis/FTIR spectroscopy, Combust. Flame 110 (1997) 239.
[4] H.E. Kissinger, Reaction kinetics in differential thermal analysis, Anal. Chem. 29 (1957) 1703.

[5] T. Ozawa, Kinetic analysis of derivative curves in thermal analysis, J. Therm. Anal. 2 (1970) 301.
[6] E.S. Freeman, B. Carroll, The thermogravimetric evaluation of the kinetics of the decomposition of calcium oxalate monohydrate, J. Phys. Chem. 62 (1958) 394.
[7] M.L. Hobbs, HMX decomposition model to characterize thermal damage, Thermochim. Acta. 384 (2002) 291.
[8] J. Kimura, N. Kubota, Thermal decomposition process of HMX, Propellants Explosives 5 (1980) 1.